Check for updates

ADVANCED FUNCTIONAL MATERIALS
www.afm-journal.de

Stretchable *p/n*-Pair Thermoelectric Fibers Based on Core (Ag)–Shell (Ag_2Se) Structure for Wearable Electronics

*Chaebeen Kwon, Sanghyeon Lee, Sungjoon Cho, Chihyeong Won, Byeonggwan Kim, Kyung-In Jang, and Taeyoon Lee**

The development of stretchable p/n-pair thermoelectric (TE) fibers holds significant promise for multifunctional wearable electronics, yet remains challenging due to complex processing and limited mechanical durability. Here, a novel strategy is presented for the facile fabrication of stretchable Ag@Ag_2Se-based TE fibers using a selective in situ chemical reduction process, eliminating the need for thermal treatment or specialized equipment. The resulting fibers feature a robust core–shell architecture, with conductive Ag cores and n-type Ag_2Se shells, achieving a Seebeck coefficient of −96.75 μV K^{-1} under 100% strain and stable electrical conductivity under 200% strain. Notably, the fibers exhibit excellent cyclic stability with $\Delta V/V_0$ maintained within 1.75% under mechanical deformation. When patterned into p/n-pair arrays through localized chemical treatment, the fibers function as efficient energy harvesters and strain/temperature sensors. Integrated into wearable platforms, these fibers demonstrate simultaneous mechanical and thermal sensing and effective energy harvesting from body heat. This work establishes a versatile platform for scalable, miniaturized, and multifunctional TE fiber systems, advancing the future of smart textiles and wearable electronics.

1. Introduction

Over the past decade, electronic devices have become smaller and evolved into wearable appliances seamlessly integrable with healthcare monitoring,[1–3] virtual and augmented reality,[4,5] and human–machine interfaces.[6–8] This progress has caused applicability and user interaction improvements and increased the demand for multifunctional fibers, which are widely used in wearable electronics as interconnects,[9–11] sensors,[12–14] and power sources.[15–17] Particular attention has been drawn to fibers based on thermoelectric (TE) materials,[18–20] which exploit the Seebeck effect to convert temperature differences into electrical power and vice versa[21,22] and therefore have a broad application scope (e.g., temperature sensors[23–25] and power sources[26–28]) and hold great promise for wearable electronics.

Recent progress in TE fibers has broadened the range of materials and methods used to develop multifunctional wearable electronics.[23,29] The rigidity of inorganic TE materials has led to a preference for their organic counterparts.[30] Previously, we incorporated Bi_2Te_3 nanoparticles (NPs) into a flexible substrate[23] to create a stretchable TE fabric capable of sensing lateral strain, normal pressure, and temperature, demonstrating the potential of inorganic TE materials in wearable platforms. However, this TE fabric contained only an *n*-type material (Bi_2Te_3) and had to be integrated with *p*-type fibers to function as a power source. This integration is challenging and can cause fiber damage, as it typically involves soldering or the use of adhesives.[31,32] The formation of continuous *p*/*n*-pair TE fibers enables the realization of true fiber multifunctionality and helps solve the abovementioned problem.[29,33] In the study of Ding et al., *p*/*n*-pair TE fibers based on single-walled carbon nanotubes were prepared using gelation extrusion[29] and woven onto a curved surface to enable sensing and energy harvesting. However, this fabrication process required specialized equipment and was therefore deemed complex and poorly accessible. Sun et al. coated carbon nanotube fibers with poly(3,4-ethylenedioxythiophene):poly(styrenesulfonate) and oleamine as *p*- and *n*-type materials, respectively, showing that the fabric woven from these *p*/*n*-pair TE fibers demonstrated a power density of 70 mW m^{-2} at a temperature difference (ΔT) of 44 K.[33] However, the coated *p*- and *n*-type materials are prone to delamination

C. Kwon, S. Lee, S. Cho, C. Won, T. Lee
Nanobio Device Laboratory
School of Electrical and Electronic Engineering
Yonsei University
50 Yonsei-ro, Seoul, Seodaemun-gu 03722, Republic of Korea
E-mail: taeyoon.lee@yonsei.ac.kr

C. Won
Andrew and Peggy Cherng Department of Medical Engineering
Division of Engineering and Applied Science
California Institute of Technology
Pasadena, CA 91125, USA

B. Kim
Department of Chemical Engineering and Applied Chemistry
Chungnam National University
99 Daehak-ro, Yuseong-gu, Daejeon 34134, Republic of Korea

K.-I. Jang
Department of Robotics Engineering
Daegu Gyeongbuk Institute of Science and Technology (DGIST)
333 Techno Jungang-daero, Daegu, Dalseong-gun 42988, Republic of Korea

The ORCID identification number(s) for the author(s) of this article can be found under https://doi.org/10.1002/adfm.202521163

© 2025 The Author(s). Advanced Functional Materials published by Wiley-VCH GmbH. This is an open access article under the terms of the Creative Commons Attribution-NonCommercial-NoDerivs License, which permits use and distribution in any medium, provided the original work is properly cited, the use is non-commercial and no modifications or adaptations are made.

DOI: 10.1002/adfm.202521163

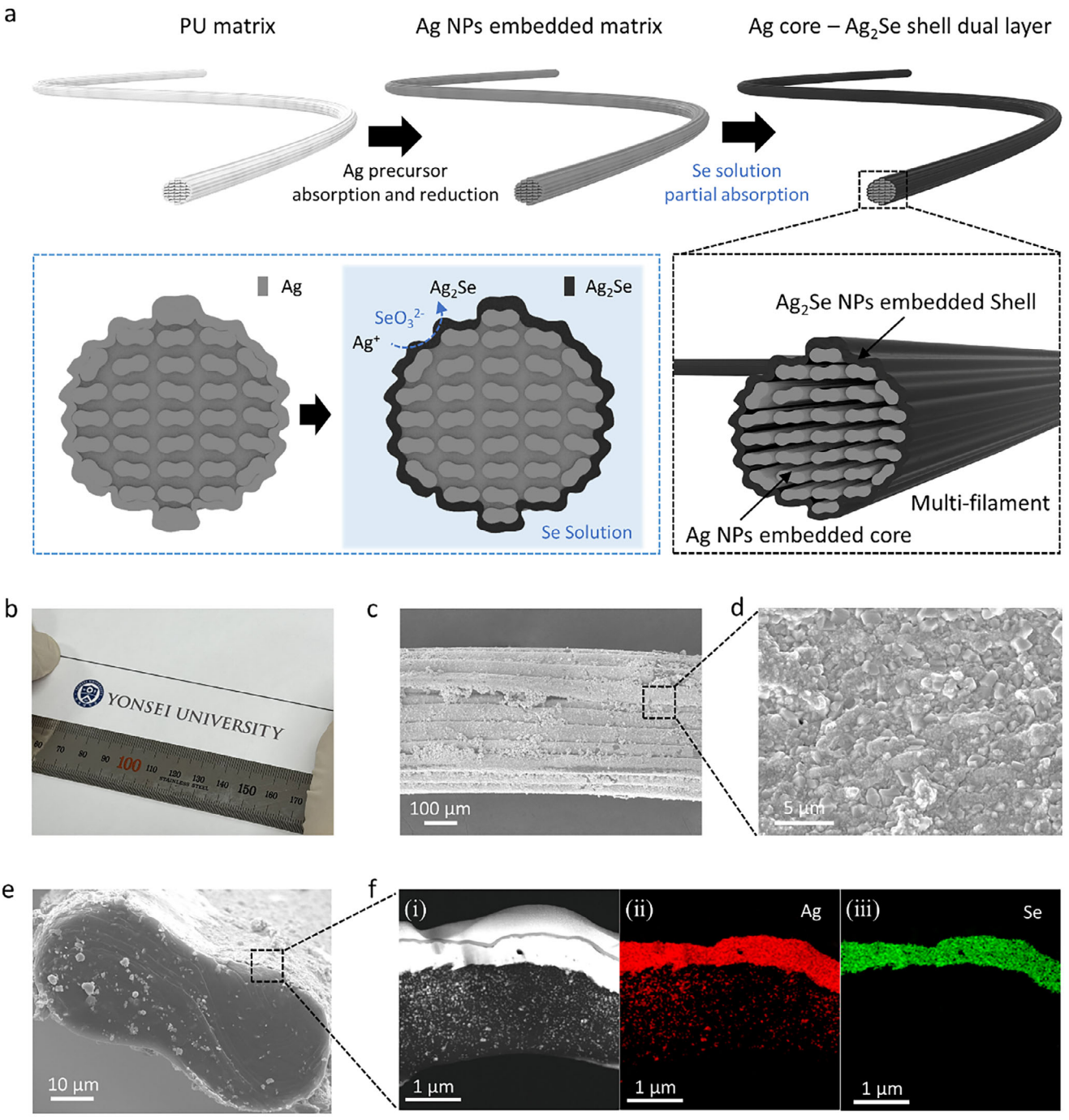

Figure 1. a) Schematic fabrication of Ag@Ag_2Se stretchable thermoelectric (TE) fibers. b) Optical and c) Cross-sectional scanning electron microscopy (SEM) images of a representative Ag@Ag_2Se stretchable TE fiber. d) High-magnification SEM image showing Ag_2Se nanoparticles grafted on the TE fiber. e) Cross-sectional SEM image of a single-filament TE fiber. f) Transmission electron microscopy (TEM) and energy-dispersive X-ray spectroscopy images of a representative TE fiber processed using a focused ion beam: i) TEM image; ii) Ag and iii) Se mappings.

upon cyclic mechanical deformation. Moreover, most *p*/*n*-pair TE fibers are based on organic TE materials, and purely stretchable *p*/*n*-pair TE fibers have not been reported, which indicates that stretchable *p*/*n*-pair TE fibers that withstanding mechanical deformation while maintaining their TE properties are required for multifunctional electronics.

Herein, stretchable Ag@Ag_2Se NP–based *p*/*n*-pair TE fibers were rapidly and easily fabricated in the absence of specialized equipment using selective in situ chemical reduction. Ag and Ag_2Se NPs were densely formed within spandex fibers to establish a robust core (Ag)–shell (Ag_2Se) structure. Owing to the durable and conductive Ag core, the fibers maintained a high

© 2025 The Author(s). Advanced Functional Materials published by Wiley-VCH GmbH

16163028, 2026, 22, Downloaded from https://advanced.onlinelibrary.wiley.com/doi/10.1002/adfm.202521163 by Daegu Gyeongbuk Institute Of, Wiley Online Library on [03/05/2026]. See the Terms and Conditions (https://onlinelibrary.wiley.com/terms-and-conditions) on Wiley Online Library for rules of use; OA articles are governed by the applicable Creative Commons License

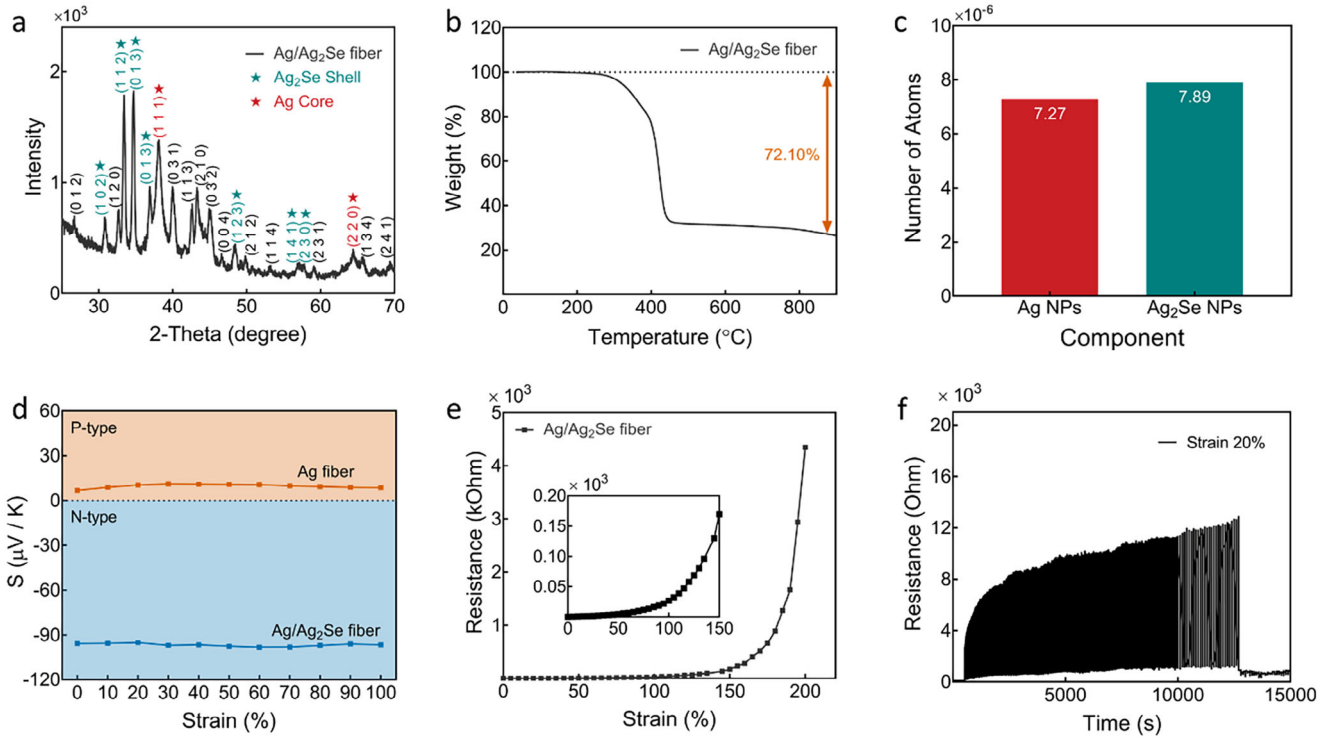

Figure 2. a) X-ray diffraction pattern and b) thermogram of Ag@Ag_2Se stretchable TE fibers. c) Ag and Ag_2Se contents of Ag@Ag_2Se stretchable TE fibers determined by inductively coupled plasma analysis. d) Seebeck coefficients of Ag and Ag@Ag_2Se stretchable TE fibers under applied strains of up to 100%. e) Resistance of Ag@Ag_2Se stretchable TE fibers under applied strains of up to 200%. f) Resistance changes of Ag@Ag_2Se stretchable TE fibers over 10 000 stretching cycles at 20% strain with a gauge length of 1 cm.

Seebeck coefficient of ≈−96.75 μV K^{-1} under tensile strains of up to 100%. Additionally, these fibers preserved their electrical conductivity under strains of up to 200% and exhibited an excellent electrical performance stability under a cyclic strain of 20%. Remarkably, fibers exposed to a temperature difference maintained a $\Delta V/V_0$ of ≤1.75% under various tensile strains, thus holding promise for wearable electronics. When woven into wearable platforms, the fibers enabled energy harvesting and strain and temperature sensing. The development of these multifunctional and miniaturized fibers represents considerable progress in wearable electronics, paving the way for innovative and integrated applications.

2. Results and Discussion

Figure 1a illustrates the fabrication of the Ag@Ag_2Se stretchable TE fibers. Pure polyurethane (PU) fibers were used as a matrix to prepare Ag NP–embedded stretchable TE fibers through Ag precursor absorption and reduction. Subsequently, the Ag NP–embedded fibers were reacted with a Se precursor solution to form an Ag_2Se shell on the surface. The hydrophilicity of PU hindered the deep penetration of the aqueous Se precursor solution (Na_2SeO_3 + Na_2SO_3 + $(NH_4)_2S_2O_3$), thus restricting Ag_2Se formation to the near-surface region. Na_2SO_3 and $(NH_4)_2S_2O_3$ reacted with the Ag NPs on the fiber surface to form Ag^+ ions, which reacted with Na_2SeO_3 to form the Ag_2Se shell. Owing to this shell, the Ag@Ag_2Se TE fibers appeared black (Figure 1b). Figure 1c presents a side-view scanning electron microscopy (SEM) image of a representative Ag@Ag_2Se TE fiber, with higher-magnification imaging revealing a surface uniformly and densely covered with Ag_2Se NPs (Figure 1d). These NPs enhanced the ability of the fibers to withstand mechanical deformation to a level superior to that achieved using traditional coating-based methods, allowing for structural integrity and performance preservation under various mechanical stresses. Furthermore, the SEM images of the multifilament configuration and the fiber under tensile strain are presented in Figure S1 (Supporting Information). The multifilament structure effectively distributes mechanical stress, while crack propagation during stretching reveals the robust core–shell (Ag–Ag_2Se) structure. These combined structural features significantly improve the fiber's mechanical and electrical stability under repeated deformation. Figure 1e shows a cross-sectional SEM image of an Ag@Ag_2Se TE fiber, and Figure 1f presents representative transmission electron microscopy (TEM) and energy-dispersive X-ray spectroscopy (EDS) images of an Ag@Ag_2Se TE fiber processed using a focused ion beam. The fiber interior contained Ag (i.e., Ag NPs; Figure 1f-(ii)) but not Se (i.e., Ag_2Se NPs; Figure 1f-(iii)). Remarkably, both Ag and Se were abundantly present on the fiber surface, representing its dense coating with Ag_2Se. The line EDS analysis shown in Figure S2 (Supporting Information) further confirms this result, indicating an Ag_2Se shell thickness of ≈0.33 μm with an underlying Ag core. The Ag_2Se shell predominantly contributes to electrical conductivity, while the Ag core serves as a ductile framework bridging microcracks and enhancing mechanical integrity.[34]

© 2025 The Author(s). Advanced Functional Materials published by Wiley-VCH GmbH

16163028, 2026, 22, Downloaded from https://advanced.onlinelibrary.wiley.com/doi/10.1002/adfm.202521163 by Daegu Gyeongbuk Institute Of, Wiley Online Library on [03/05/2026]. See the Terms and Conditions (https://onlinelibrary.wiley.com/terms-and-conditions) on Wiley Online Library for rules of use; OA articles are governed by the applicable Creative Commons License

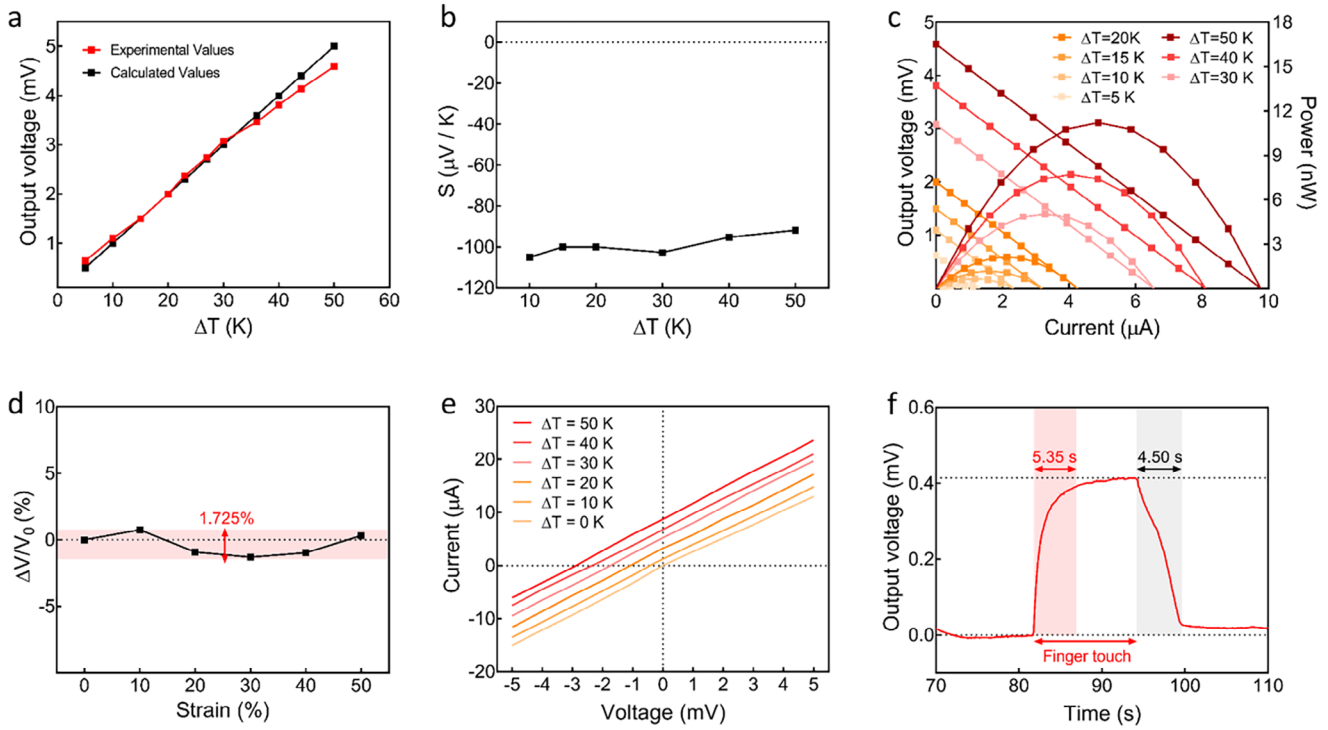

Figure 3. a) Experimental and calculated output voltages of Ag@Ag_2Se stretchable TE fibers at various temperature differences (ΔT). b) Seebeck coefficients of Ag@Ag_2Se stretchable TE fibers at various ΔT. c) Current-dependent output voltage and power of Ag@Ag_2Se stretchable TE fibers at various ΔT. d) Relative changes in the output voltage of Ag@Ag_2Se stretchable TE fibers under different strains. e) Current–voltage curves of Ag@Ag_2Se stretchable TE fibers measured at ΔT = 0–50 K. f) Output voltage changes of Ag@Ag_2Se stretchable TE fibers in response to being touched by a finger.

The X-ray diffraction patterns of the Ag@Ag_2Se TE fibers (**Figure 2a**) revealed the presence of crystalline Ag ((111) and (220) peaks) and Ag_2Se ((102), (112), (013), (123), (141), and (230) peaks),[35,36] in agreement with the Ag core–Ag_2Se shell structure. Based on the results of thermogravimetric analysis (TGA; Figure 2b), the combined Ag and Ag_2Se loading was determined as ≈27.9 wt.% with respect to PU. The Ag:Ag_2Se molar ratio was determined as 7.27:7.89 using inductively coupled plasma analysis (Figure 2c). Figure 2d shows the Seebeck coefficients of the Ag and Ag@Ag_2Se TE fibers as functions of the applied tensile strain (up to 100% in steps of 10%). In the former case, the Seebeck coefficient was constant (22489.66 μV K^{-1}) at all strains, with its positive value indicating the *p*-type–like TE response of the Ag fiber. In the latter case, the Seebeck coefficient was also constant (≈−96.75 μV K^{-1}), indicating the *n*-type behavior of Ag_2Se despite its low loading suggested by the data in Figure 2a,b. The Seebeck coefficient of the Ag@Ag_2Se stretchable TE fibers remained nearly unchanged under 100% strain. This behavior can be explained by the Mott relation, which indicates that S depends on the energy derivative of the electronic conductivity near the Fermi level rather than on geometric factors. Although tensile strain elongates the conduction path and slightly reduces the absolute conductivity, the ductile Ag core maintains electronic percolation across Ag_2Se grains, preventing disruption of the underlying energy-dependent transport. In addition, most of the applied stress is absorbed by the elastic spandex and the Ag framework, minimizing band-structure distortion in the Ag_2Se shell. To further confirm this interpretation, Ag_2Se shell thickness was adjusted by varying the concentration of the Ag precursor solution (Figure S3, Supporting Information)). Fibers prepared with 30 wt.% precursor exhibited the most stable Seebeck coefficient under strain, suggesting that an optimal Ag/Ag_2Se ratio ensures balanced mechanical compliance and electronic stability. The resistance of the Ag@Ag_2Se TE fibers increased with the increasing tensile strain, while the overall electrical transport remained stable under tensile strains of up to 200% (Figure 2e). Although tensile stretching reduces the effective cross-sectional area of the fibers, resistance was used here as a representative metric to illustrate the strain-dependent electrical trend. Moreover, these fibers did not exhibit notable electrical property deterioration during 10 000 stretching cycles at a strain of 20% with a gauge length of 1 cm (Figure 2f).

Figure 3a presents the experimental and calculated output voltages of the Ag@Ag_2Se TE fibers at various ΔT. The experimental output voltage linearly increased with the increasing ΔT, closely matching the calculated values. This linearity was attributed to the marginal effect of ΔT on the Seebeck coefficient (Figure 3b). Figure 3c shows the current-dependent output voltage and power of the Ag@Ag_2Se TE fibers at various ΔT, showing that the maximum power at ΔT = 5, 10, 15, 20, 30, 40, and 50 K equaled ≈0.21, 0.64, 1.20, 2.13, 5.05, 7.72, and 11.21 nW, respectively. The $\Delta V/V_0$ of the Ag@Ag_2Se TE fibers at a given ΔT remained within 1.75% under various tensile strains, highlighting the suitability of this material for wearable electronics (Figure 3d). Figure 3e shows the current–voltage (*I*–*V*) curves of the Ag@Ag_2Se TE fibers at ΔT = 0–50 K, demonstrating their temperature-sensing

© 2025 The Author(s). Advanced Functional Materials published by Wiley-VCH GmbH

16163028, 2026, 22, Downloaded from https://advanced.onlinelibrary.wiley.com/doi/10.1002/adfm.202521163 by Daegu Gyeongbuk Institute Of, Wiley Online Library on [03/05/2026]. See the Terms and Conditions (https://onlinelibrary.wiley.com/terms-and-conditions) on Wiley Online Library for rules of use; OA articles are governed by the applicable Creative Commons License

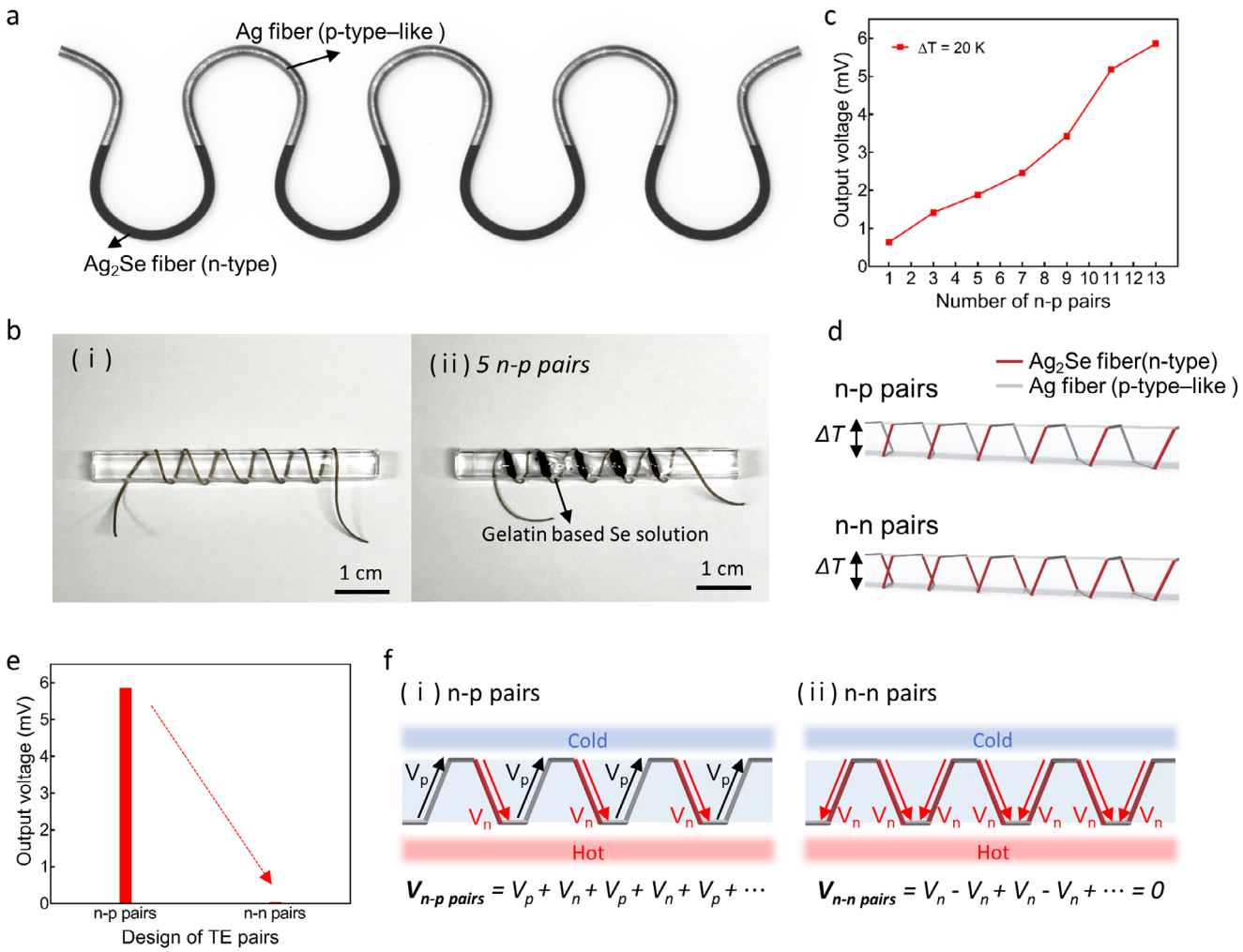

Figure 4. a) Schematic of *p*/*n*-pair Ag@Ag_2Se stretchable TE fibers. b-i) Image of five turns of Ag fiber wound around an acrylic bar. b-ii) Image showing the selective chemical modification of the Ag fiber using a gelatin-based Se solution. c) Output voltages of *p*/*n*-pair Ag@Ag_2Se stretchable TE fibers with varying numbers of *p*/*n* pairs. d) Design of *p*/*n* and *n*/*n* pairs in Ag@Ag_2Se TE fibers. e) Output voltages of *p*/*n*- and *n*/*n*-pair TE fibers at a given ΔT. f-i) Enhanced output voltage in the *p*/*n* pairs of the TE fiber aligned with the heat flow. f-ii) Reduced output voltage in the *n*/*n* pairs of the TE fiber.

capability. The absolute values of the *x*-axis intercepts indicate the output voltages due to the Seebeck effect, equaling 0.39, 1.03, 1.65, 2.41, and 2.88 mV at ΔT = 10, 20, 30, 40, and 50 K, respectively. With the increasing ΔT, the *I*–*V* curves shifted upward without a change in slope, which indicated that fiber resistance was not affected by ΔT. When touched by a finger, the Ag@Ag_2Se TE fibers experienced an output voltage change due to heating, with the response and recovery times equaling 5.35 and 4.50 s, respectively (Figure 3f). These times were defined as those required for the output voltage to stabilize and recover to the baseline value (0 mV), respectively. The thermal response and recovery test using the Ag@Ag2Se TE fibers is provided in Movie S1 (Supporting Information).

Figure 4a illustrates the structure of *p*/*n*-pair stretchable Ag@Ag_2Se TE fibers prepared by applying a gelatin-based Se precursor solution to the targeted regions of Ag stretchable fibers. In this case, the original aqueous Se precursor solution was supplemented with gelatin to increase viscosity and prevent unnecessary diffusion. The Ag shell in the treated region transformed into an Ag_2Se shell, as described above. Figure 4b-(i) shows an image of five turns of an Ag fiber wound around an acrylic bar. The Se precursor solution was applied to the front side of the fiber to form continuous *p*/*n* pairs, with Ag fibers and Ag_2Se fibers acting as the *p*-type–like and *n*-type TE components, respectively (Figure 4b-(ii)). At a ΔT of 20 K, the output voltage of the *p*/*n*-pair Ag@Ag_2Se TE fibers increased with the increasing pair number (Figure 4c; Movie S2, Supporting Information). Figure 4d illustrates the design of *p*/*n*- and *n*/*n*-pair Ag@Ag_2Se TE fibers. Under an applied heat flow, the output voltages of 11-turn *p*/*n*- and *n*/*n*-pair TE fibers were 5.86 and ≈0 mV, respectively (Figure 4e). Each Ag_2Se segment develops a thermovoltage V_n , with the hot side being positive and the cold side negative, whereas each Ag segment develops a thermovoltage V_p, with the cold side positive and the hot side negative. In the *p*/*n*-pair TE fibers, the output voltages of the segments act synergistically and are summed as (V_p+V_n+V_p+V_n ...). In contrast, in the *n*/*n*-pair TE fibers, the voltages canceled each other (V_n–V_n +V_n –V_n ...) due to their opposing directionality. Because the Ag segments arranged at hot–hot

© 2025 The Author(s). Advanced Functional Materials published by Wiley-VCH GmbH

16163028, 2026, 22, Downloaded from https://advanced.onlinelibrary.wiley.com/doi/10.1002/adfm.202521163 by Daegu Gyeongbuk Institute Of, Wiley Online Library on [03/05/2026]. See the Terms and Conditions (https://onlinelibrary.wiley.com/terms-and-conditions) on Wiley Online Library for rules of use; OA articles are governed by the applicable Creative Commons License

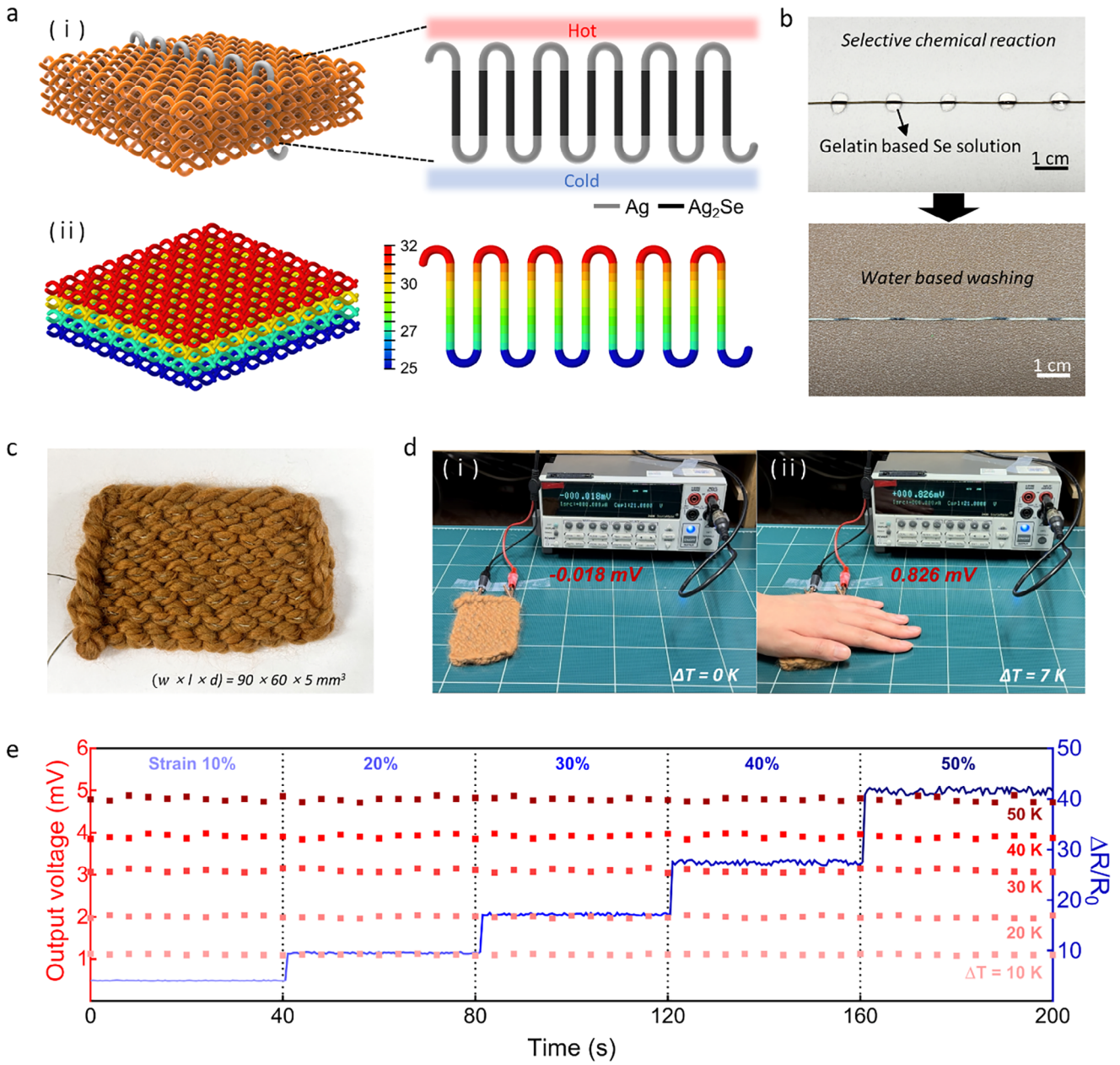

Figure 5. a) i) Schematic integration of Ag@Ag_2Se stretchable TE fibers into a woven fabric. ii) Temperature distribution of a TE fiber embedded into the fabric, demonstrating the thermal gradient across the system. b) Selective chemical reaction–based fabrication of 1D *p*/*n*-pair Ag@Ag_2Se stretchable TE fibers. c) Application of *p*/*n*-pair Ag@Ag_2Se stretchable TE fibers in wearable platforms achieved through weaving. d) Utility demonstration of a wearable device for harvesting the thermal energy of the body ($\Delta T = 7$ K). e) Performance of Ag@Ag_2Se stretchable TE fibers for simultaneous temperature and strain sensing.

or cold–cold junctions do not experience a temperature gradient, their contribution to the thermovoltage is effectively zero. This indicates the importance of aligning *p*/*n* pairs with the heat flow for maximizing the energy harvesting efficiency (Figure 4f). Therefore, the selective chemical reaction–based pair design enhanced the flexibility of TE fiber pair structures, enabling the effective design of power sources for various heat flows.

The chemical engineering of the *p*/*n* components of the TE fibers allows one to precisely control the spacing between the TE components without using complicated equipment and thus makes them adaptable to the thermal flux of any wearable platform, facilitating the integration of TE fibers into wearable platforms. **Figure** 5a-(i) illustrates a wearable platform with incorporated *p*/*n*-pair Ag@Ag_2Se TE fibers, and Figure 5a-(ii) presents the temperature distribution of this platform for top and bottom temperatures of 32 and 25 °C, respectively. Aligning the Ag_2Se component in the direction of the heat flux facilitated energy harvesting, which underscores the benefits of using the

© 2025 The Author(s). Advanced Functional Materials published by Wiley-VCH GmbH

16163028, 2026, 22, Downloaded from https://advanced.onlinelibrary.wiley.com/doi/10.1002/adfm.202521163 by Daegu Gyeongbuk Institute Of, Wiley Online Library on [03/05/2026]. See the Terms and Conditions (https://onlinelibrary.wiley.com/terms-and-conditions) on Wiley Online Library for rules of use; OA articles are governed by the applicable Creative Commons License

chemically selective reaction. The spacing between the TE components was easy to control, which is particularly important for wearable applications, ensuring a perfect fit with the applied wearable platforms. Figure 5b illustrates the fabrication of 1D *p*/*n*-pair Ag@Ag_2Se stretchable TE fibers through the selective chemical reaction. The gelatin-based Se precursor solution was applied to the targeted region, which enabled precise control over the intervals between the *p* and *n* components. After the chemical reaction, this solution was removed by washing with deionized (DI) water. Figure 5c shows an optical image of a wearable platform incorporating the abovementioned TE fibers, revealing their seamless blending into the textile background. When touched by the palm, this integrated textile generated an output voltage in response to a ΔT of ≈7 K (Figure 5d), which demonstrates the possibility of harvesting the thermal energy of the body in wearable applications. The developed system simultaneously detected temperature differences and tensile strains (Figure 5e). The output voltage increased with the increasing ΔT because of the Seebeck effect, and the relative resistance linearly increased with the increasing tensile strain because of the intrinsic piezoresistance of Ag_2Se NPs. Importantly, the output voltage and relative resistance changes were independent of each other, which ensured the precise and simultaneous detection of thermal and mechanical stimuli. A benchmarking comparison shown in Table S1 (Supporting Information) highlights that the present Ag@Ag_2Se stretchable TE fibers represent the all-inorganic, stretchable single-fiber *p*/*n*-pair system, uniquely combining 200% stretchability, durable electrical stability, and simple, equipment-free fabrication.

3. Conclusion

Ag@Ag_2Se NP–based *p*/*n*-pair stretchable TE fibers were fabricated using an in situ chemical reaction. The Ag and Ag_2Se NPs were densely formed within spandex fibers to create a robust core (Ag)–shell (Ag_2Se) structure. This structure allowed the TE fibers to maintain a high Seebeck coefficient of ≈−96.75 μV K^{-1} under tensile strains of up to 100%, preserve electrical conductivity under strains of up to 200%, and exhibit an excellent electrical performance stability upon cyclic stretching at a strain of 20%. The $\Delta V/V_0$ of the fibers at a fixed ΔT remained within 1.75% under various tensile strains, highlighting their suitability for wearable electronics. The selective chemical reaction enabled the easy and rapid fabrication of these fibers without the need for specialized equipment. When woven into wearable platforms, the fibers acted as strain and temperature sensors, as well as energy harvesters, substantially advancing the field of wearable electronics.

4. Experimental Section

Fabrication of Ag@Ag_2Se Stretchable TE Fibers: Creora Power Fit PU-based spandex fibers (Hyosung) were immersed into an ethanolic solution of $AgCF_3COO$ (30 wt.%) for 20 min, and ethanol was subsequently evaporated over 5 min at room temperature. The impregnated fibers were treated with a 50 vol% solution of hydrazine hydrate in ethanol for 3 min, rinsed with deionized (DI) water to eliminate residual hydrazine hydrate, and left to dry. The resulting Ag stretchable fibers were soaked in the Se precursor solution (5 wt.% Na_2SeO_3, 15 wt.% Na_2SO_3, and 30 wt.% $(NH_4)_2S_2O_3$ in DI water) for 2 h and rinsed with DI water to afford Ag@Ag_2Se stretchable TE fibers. In this system, Na_2SeO_3 serves as the selenium source, while Na_2SO_3 and $(NH_4)_2S_2O_3$ function as reducing agents that provide electrons to convert Se(IV) species into selenide anions (Se^{2-}). The generated Se^{2-} ions subsequently react with the surface Ag NPs to form an Ag_2Se shell around the metallic Ag core.

Characterization: Imaging was performed using field-emission SEM (7610F-Plus, JEOL) and TEM-EDS (JEM-F200, JEOL). TGA was performed using a thermal analyzer (Q50, TA Instruments). Electrical and mechanical properties were probed using a source meter (B2901A, Keysight Technologies) and a force transducer (S2M, HBM), respectively. Stretching tests were performed using a customized machine equipped with a motorized *x*-axis stage (X-translation stage, Jaeil Optical Corp). TE properties were examined using a custom-built machine. Thermal analysis was conducted using Hypermesh (Altair).

Supporting Information

Supporting Information is available from the Wiley Online Library or from the author.

Acknowledgements

C.K. and S.L. contributed equally to this work. This work was supported by the National Research Foundation of Korea (NRF) grant funded by the Korea government (MSIT) (No. RS-2023-00234581). This work was supported by the Technology Innovation Program (RS-2025-02304448, Development of a patient-tailored, cervical-worn wearable electronic drug based on multiple external stimulation therapy for dysphagia rehabilitation) funded By the Ministry of Trade Industry&Energy (MOTIE,Korea).

Conflict of Interest

The authors declare no conflict of interest.

Data Availability Statement

The data that support the findings of this study are available on request from the corresponding author. The data are not publicly available due to privacy or ethical restrictions.

Keywords

Ag@Ag_2Se core–shell structure, energy harvesting, strain and temperature sensing, stretchable thermoelectric fibers, wearable electronics

Received: August 12, 2025
Revised: October 11, 2025
Published online: November 22, 2025

[1] X. Chen, Y. He, M. Tian, L. Qu, T. Fan, J. Miao, *Small* **2024**, *20*, 2308404.
[2] H. Kim, J. Lee, U. Heo, D. K. Jayashankar, K. C. Agno, Y. Kim, C. Y. Kim, Y. Oh, S. H. Byun, B. Choi, H. Jeong, W. H. Yeo, Z. Li, S. Park, J. Xiao, J. Kim, J. W. Jeong, *Sci. Adv.* **2024**, *10*, adk5260.
[3] G. Tian, W. Deng, T. Yang, J. Zhang, T. Xu, D. Xiong, B. Lan, S. Wang, Y. Sun, Y. Ao, L. Huang, Y. Liu, X. Li, L. Jin, W. Yang, *Adv. Mater.* **2024**, *36*, 2313612.

© 2025 The Author(s). Advanced Functional Materials published by Wiley-VCH GmbH

16163028, 2026, 22, Downloaded from https://advanced.onlinelibrary.wiley.com/doi/10.1002/adfm.202521163 by Daegu Gyeongbuk Institute Of, Wiley Online Library on [03/05/2026]. See the Terms and Conditions (https://onlinelibrary.wiley.com/terms-and-conditions) on Wiley Online Library for rules of use; OA articles are governed by the applicable Creative Commons License

[4] F. Wen, Z. Zhang, T. He, C. Lee, *Nat. Commun.* **2021**, *12*, 5378.
[5] L. Li, S. Zhao, W. Ran, Z. Li, Y. Yan, B. Zhong, Z. Lou, L. Wang, G. Shen, *Nat. Commun.* **2022**, *13*, 5975.
[6] S. Kim, J. Jang, K. Kang, S. Jin, H. Choi, D. Son, M. Shin, *Adv. Mater.* **2023**, *35*, 2307070.
[7] Z. Sun, M. Zhu, X. Shan, C. Lee, *Nat. Commun.* **2022**, *13*, 2453.
[8] C. Hou, G. Tai, Y. Liu, R. Liu, X. Liang, Z. Wu, Z. Wu, *Nano Energy* **2022**, *97*, 107189.
[9] X. Cheng, H. Gao, X. Tian, D. Wu, P. Lv, S. S. Yoon, J. Yang, Q. Wei, *Nano Energy* **2024**, *125*, 109501.
[10] T. Zhou, C. Cao, S. Yuan, Z. Wang, Q. Zhu, H. Zhang, J. Yan, F. Liu, T. Xiong, Q. Cheng, L. Wei, *Adv. Mater.* **2023**, *35*, 2305807.
[11] J. S. Marion, N. Gupta, H. Cheung, K. Monir, P. Anikeeva, Y. Fink, *Adv. Mater.* **2022**, *34*, 2201081.
[12] W. Fan, R. Lei, H. Dou, Z. Wu, L. Lu, S. Wang, X. Liu, W. Chen, M. Rezakazemi, T. M. Aminabhavi, Y. Li, S. Ge, *Nat. Commun.* **2024**, *15*, 3509.
[13] K. Wang, X. Sun, S. Cheng, Y. Cheng, K. Huang, R. Liu, H. Yuan, W. Li, F. Liang, Y. Yang, F. Yang, K. Zheng, Z. Liang, C. Tu, M. Liu, M. Ma, Y. Ge, M. Jian, W. Yin, Y. Qi, Z. Liu, *Nat. Commun.* **2024**, *15*, 5040.
[14] Y. Lu, H. Zhang, Y. Zhao, H. Liu, Z. Nie, F. Xu, J. Zhu, W. Huang, *Adv. Mater.* **2024**, *36*, 2310613.
[15] R. Garg, A. Majhi, N. P., N. R. Patra, R. Barve, K. Parida, *Adv. Mater.* **2024**, *34*, 2401593.
[16] C. Zhi, H. Wu, J. Hu, *Nano Energy* **2024**, *127*, 109705.
[17] Y. Jung, S. Jeong, J. Ahn, J. Lee, S. H. Ko, *Small* **2024**, *20*, 2304338.
[18] R. Sarabia-Riquelme, L. E. Noble, P. A. Espejo, Z. Ke, K. R. Graham, J. Mei, A. F. Paterson, M. C. Weisenberger, *Adv. Funct. Mater.* **2024**, *34*, 2311379.
[19] J. Yang, Y. Pu, H. Yu, D. Ye, X. Liu, J. H. Xin, *Small* **2023**, *19*, 2304529.
[20] M. Sun, G. Tang, H. Wang, T. Zhang, P. Zhang, B. Han, M. Yang, H. Zhang, Y. Chen, J. Chen, Q. Zhu, J. Li, D. Chen, J. Gan, Q. Qian, Z. Yang, *Adv. Mater.* **2022**, *34*, 2202942.
[21] Y. Fu, S. Kang, G. Xiang, C. Su, C. Gao, L. Tan, H. Gu, S. Wang, Z. Zheng, S. Dai, C. Lin, *Adv. Mater.* **2024**, *36*, 2313101.
[22] J. Liang, J. Liu, P. Qiu, C. Ming, Z. Zhou, Z. Gao, K. Zhao, L. Chen, X. Shi, *Nat. Commun.* **2023**, *14*, 8442.
[23] C. Kwon, S. Lee, C. Won, K. H. Lee, M. Kim, J. Lee, S.-J. Yang, M. Lee, S. Lee, K. Yoon, S. Cho, T. Lee, *Adv. Funct. Mater.* **2023**, *33*, 2300092.
[24] H. Chen, H. Xu, M. Luo, W. Wang, X. Qing, Y. Lu, Q. Liu, L. Yang, W. Zhong, M. Li, D. Wang, *ACS Appl. Mater. Interfaces* **2023**, *15*, 20346.
[25] X. Xia, Q. Zhang, W. Zhou, J. Mei, Z. Xiao, W. Xi, Y. Wang, S. Xie, W. Zhou, *Small* **2021**, *17*, 2102825.
[26] J. Ren, Z. Liu, Q. Li, L. Chen, J. Gong, H. Wang, Y. Li, J. Qu, R. Niu, *ACS Appl. Mater. Interfaces* **2024**, *16*, 18855.
[27] M. Li, H. Xu, M. Luo, X. Qing, W. Wang, W. Zhong, Q. Liu, Y. Wang, L. Yang, X. Zhu, D. Wang, *Chem. Eng. J.* **2024**, *485*, 149784.
[28] J. Li, B. Xia, X. Xiao, Z. Huang, J. Yin, Y. Jiang, S. Wang, H. Gao, Q. Shi, Y. Xie, J. Chen, *ACS Nano* **2023**, *19*, 19232.
[29] T. Ding, K. H. Chan, Y. Zhou, X. Q. Wang, Y. Cheng, T. Li, G. W. Ho, *Nat. Commun.* **2020**, *11*, 1620.
[30] C. Xu, Y. Sun, J. Zhang, W. Xu, H. Tian, *Adv. Energy Mater.* **2022**, *12*, 2200157.
[31] A. A. Simegnaw, B. Malengier, M. Getnet, L. Van Langenhove, *Text. Res. J.* **2023**, *93*, 4068.
[32] K. Garbacz, L. Stagun, S. Rotzler, M. Semenec, M. von Krshiwoblozki, *Proceedings* **2021**, *1*, 5.
[33] T. Sun, B. Zhou, Q. Zheng, L. Wang, W. Jiang, G. J. Snyder, *Nat. Commun.* **2020**, *11*, 572.
[34] J. Lee, S. Shin, S. Lee, J. Song, S. Kang, H. Han, S. Kim, S. Kim, J. Seo, D. Kim, T. Lee, *ACS Nano* **2018**, *12*, 4259.
[35] S. Sunaryono, A. Rachmawati, C. I. Yogihati, H. Susanto, A. Taufiq, N. Mufti, *Polym. Bull.* **2022**, *79*, 555.
[36] Y. Yan, X. Qian, H. Xu, J. Yin, Z. Zhu, *Inorg. Chem. Commun.* **2003**, *6*, 34.

© 2025 The Author(s). Advanced Functional Materials published by Wiley-VCH GmbH

16163028, 2026, 22, Downloaded from https://advanced.onlinelibrary.wiley.com/doi/10.1002/adfm.202521163 by Daegu Gyeongbuk Institute Of, Wiley Online Library on [03/05/2026]. See the Terms and Conditions (https://onlinelibrary.wiley.com/terms-and-conditions) on Wiley Online Library for rules of use; OA articles are governed by the applicable Creative Commons License